ANNUAL REVIEWS

Annual Review of Nuclear and Particle Science

Covariant Density Functional Theory in Nuclear Physics and Astrophysics

Junjie Yang and J. Piekarewicz

Department of Physics, Florida State University, Tallahassee, Florida 32306-4350, USA; email: jpiekarewicz@fsu.edu

Annu. Rev. Nucl. Part. Sci. 2020. 70:21–41

First published as a Review in Advance on June 2, 2020

The *Annual Review of Nuclear and Particle Science* is online at nucl.annualreviews.org

https://doi.org/10.1146/annurev-nucl-101918-023608

Keywords

density functional theory, equation of state, neutron stars

Abstract

How does subatomic matter organize itself? Neutron stars are cosmic laboratories uniquely poised to answer this fundamental question that lies at the heart of nuclear science. Newly commissioned rare isotope facilities, telescopes operating across the entire electromagnetic spectrum, and ever more sensitive gravitational wave detectors will probe the properties of neutron-rich matter with unprecedented precision over an enormous range of densities. A coordinated effort between observation, experiment, and theoretical research is of paramount importance for realizing the full potential of these investments. Theoretical nuclear physics provides valuable insights into the properties of neutron-rich matter in regimes that are not presently accessible to experiment or observation. In particular, nuclear density functional theory is likely the only tractable framework that can bridge the entire nuclear landscape by connecting finite nuclei to neutron stars. This compelling connection is the main scope of the present review.

Contents

1. INTRODUCTION

Nuclear science is poised to enter a period of transformational changes driven by the upgrade and commissioning of state-of-the-art experimental and observational facilities. As we embark on this new journey of discovery, nuclear theory will play a critical role in guiding new experimental programs and in predicting the properties of nuclear matter in regimes that will remain inaccessible to experiment and observation. With unparalleled depth and breadth, nuclear science is driven by the quest to answer fundamental questions ranging from the quark–gluon structure of hadronic matter to the synthesis of heavy elements in cataclysmic stellar explosions (1). In this review, we focus on the critical role that density functional theory (DFT) plays in our understanding of a variety of nuclear phenomena that range from the structure and dynamics of exotic nuclei to the fascinating properties of neutron stars. Remarkable advances in theoretical nuclear physics have propelled traditional wave function methods to such heights that highly accurate predictions of the properties of small- to medium-sized nuclei are now routine (see References 2–5 and references contained therein). Such ab initio approaches provide meaningful benchmarks for the development of reliable energy density functionals (EDFs), which can then be applied to larger nuclear systems. Indeed, this powerful connection between ab initio approaches and DFT is one of the main motivations behind the ^{48}Ca Radius Experiment (CREX) at Jefferson Lab (6, 7). Multiple paths exist to improve the performance of nuclear EDFs and transform them into proper effective field theories. For a recent perspective on how to approach this challenging task, readers are referred to Reference 8 and references contained therein.

DFT is a powerful technique developed by Kohn and collaborators (9, 10) in the mid-1960s to understand the electronic structure of complex many-body systems and for which Kohn was recognized with the 1998 Nobel Prize in Chemistry (11). Today, DFT is widely used in chemistry as well as in many areas of physics (12–15). In its original application to electronic structure, Hohenberg & Kohn (9) assumed the validity of the Born–Oppenheimer approximation, which defines the many-body Hamiltonian in terms of a conventional kinetic energy contribution, a two-body potential that accounts for the electronic repulsion, and a one-body attractive potential provided by the stationary nuclei. Given that in the Born–Oppenheimer approximation the position of the heavy nucleus is assumed to be fixed, this last term is commonly referred to as the external potential. DFT is firmly rooted in the two Hohenberg–Kohn (HK) theorems, which state (*a*) that a one-to-one correspondence exists between the one-body electronic density and a suitable external potential and (*b*) that an EDF exists that, upon functional minimization, yields both the exact ground-state energy and one-body density of the complicated many-body system

(9). Essentially, the HK theorems establish a remarkable and subtle result: The exact ground-state energy of the complicated many-body system may be obtained from minimizing a suitable EDF that only depends on the one-body density. Perhaps the greatest virtue of DFT is that it shifts the focus from the complicated many-body wave function that depends on $3N$ spatial coordinates (for an N-particle system) to the much more intuitive one-body density that depends only on three coordinates. By doing so, DFT not only reduces drastically the complexity of the problem but also invites physical insights into the construction of the functional. This is particularly relevant because the HK theorem is an existence theorem that offers no guidance on how to construct the appropriate EDF. This limitation presents a serious challenge to the implementation because no accurate representation of the kinetic energy part of the EDF exists.

In an effort to mitigate this problem, and inspired by Hartree–Fock theory, Kohn & Sham (10) replaced the complex interacting system with an equivalent system of noninteracting electrons moving in a suitably generated external potential. The word equivalent is used to indicate that the Kohn–Sham (KS) potential must be sophisticated enough to reproduce the exact one-body density of the interacting system. Thus, while the KS equations for the fictitious system closely resemble the structure of the Hartree equations, they differ by the presence of an exchange-correlation term that ensures that its density is identical to that of the interacting system. In essence, the KS approach bypasses the search for an accurate EDF and, instead, employs a complex exchange-correlation potential. Nevertheless, the reformulation of the DFT problem in terms of one-particle orbitals has several advantages. First, unlike orbital-free DFT, in which the kinetic energy functional is unknown and complex, the kinetic energy term for the fictitious system is known. Second, the computational cost is minimal as it increases linearly with the number of occupied orbitals. Third, the construction of the one-body density involves a simple sum over the occupied single-particle orbitals. Finally, self-consistent problems of this kind have been around for almost a century, so efficient and robust methods for their solution abound. Self-consistency is demanded because the one-body density depends on the single-particle orbitals, which in turn are solutions of a Schrödinger (or Dirac) equation in the presence of a density-dependent KS potential.

After this historical interlude, it is appropriate to ask how DFT can be extended from the electronic sector to the nuclear domain. Unfortunately, the answer is far from obvious (8). One immediate difficulty concerns the one-to-one correspondence between the one-body density and the external potential, a concept that lies at the heart of DFT. As self-bound, many-body systems, atomic nuclei are not subjected to any external potential. Hence, within the scope of the original orbital-free DFT of Hohenberg & Kohn (9), the generalization to nuclear physics is unclear. Yet, within the mean-field-like KS paradigm, some similarities emerge. After all, mean-field theory has been an integral part of nuclear theory for many decades (see Reference 16 and references contained therein). Although the external potential is germane to the KS formalism, could one simply regard the nuclear mean field as the KS potential without the all-important external potential? Regrettably, this is not the case, mainly because of the necessity of the complicated exchange-correlation potential that is essential to reproduce the exact ground-state energy. Indeed, neglecting the exchange-correlation potential reduces the KS equations to the much simpler set of Hartree equations (11). However, in the context of nuclear physics, it is well known that a Hartree potential computed from the convolution of the bare nucleon–nucleon interaction with the nuclear density provides a poor description of the properties of atomic nuclei (16). To overcome this problem, effective density-dependent forces were developed by Skyrme (17, 18) almost a decade before the inception of DFT. In particular, part of the success of the Skyrme interaction relies on the existence of powerful relations connecting the (isoscalar) parameters of the model to various bulk properties of infinite nuclear matter, such as the saturation density, binding

energy per nucleon, and incompressibility coefficient (19, 20). In this manner, important features of the nuclear dynamics are directly encoded into the parameters of the model. Reminiscent of the Hartree–Fock approach—or the more modern KS approach—the resulting single-particle equations of motion are derived from functional minimization of a properly defined Skyrme EDF. Thus, while the notion of a nuclear mean-field potential remains essential, its connection to the underlying (or "bare") nucleon–nucleon interaction has been lost. Indeed, present-day nuclear EDFs are largely empirical because the parameters of the model have no direct connection to the underlying nucleon–nucleon interaction, which is often calibrated using deuteron properties and phase shifts. In DFT, the model parameters are fitted to selected properties of atomic nuclei. One often justifies empirical EDFs by invoking the HK theorems, which as existence theorems provide no guidance on how to construct the functional. Nevertheless, significant advances have been made over the last decade to mitigate the reliance on empirical EDFs in favor of more fundamental ones (for an extensive review, see Reference 15 and references contained therein). In parallel, much effort has been devoted to the construction of a Universal Nuclear Energy Density Functional with the aim of achieving a comprehensive understanding of finite nuclei across the entire nuclear landscape (21–25).

In this review, we continue to rely on empirical EDFs but within the context of covariant DFT. Our motivation for this generalization is mostly pragmatic; we seek a unified approach that can simultaneously describe the dynamics of finite nuclei and neutron stars—systems with natural-length scales that differ by 18 orders of magnitude. We aim to build high-quality functionals that yield an accurate description of the properties of finite nuclei and generate an equation of state (EoS) that is consistent with known neutron star properties while providing a Lorentz covariant extrapolation to dense matter. In the case of finite nuclei, an important goal is to compute not only ground-state properties but also the linear response of the ground state to a variety of probes. In this context, DFT continues to provide an ideal framework. Indeed, given the variational nature of DFT, small oscillations around the variational minimum encapsulate the linear response of the ground state to weak external perturbations. However, care must be exercised in employing a residual interaction that is consistent with the one employed to generate the ground state. Only then can one ensure that important symmetries and conservation laws are properly enforced (26–29). Finally, given that some of the observables of interest require extrapolations into regions that are inaccessible in the laboratory, we aim when possible to supplement our predictions with theoretical uncertainties (23, 30–37). Such adjustments can now be done routinely because the calibration of the EDF produces a statistically robust covariant matrix.

Exploring the synergy between nuclear physics and astrophysics has always been a core mission of nuclear science. In the particular context of neutron stars, the EoS prescribed by the underlying DFT becomes essential in the description of the structure and dynamics of these fascinating compact objects. The powerful connection between nuclear physics and astrophysics has been strengthened further with the first direct detection of gravitational waves from the binary neutron star merger GW170817 (38). In one clean sweep, GW170817 confirmed the long-held belief that short gamma ray bursts are associated with the merger of two neutron stars, identified the leftover kilonova as the electromagnetic transient powered by the radioactive decay of the heavy elements synthesized in the rapid neutron-capture process (39–42), and provided stringent constraints on the EoS (43–51). Assessing the impact of this historic discovery is an important component of this review.

We have organized the review as follows. In Section 2, we start by discussing the class of covariant density functionals that are considered in this work. We then introduce the associated set of equations that must be solved to obtain KS orbitals and ground-state densities. Next, we illustrate how to compute the nuclear matter EoS using the same exact covariant EDFs (note that the

EoS is the sole ingredient required to solve the equations of hydrostatic equilibrium from which several neutron star properties are extracted). Having developed the formalism, we then move to Section 3, in which our predictions are discussed with special emphasis on those observables that are difficult to probe under present laboratory conditions, either because of the large neutron excess or because of the very high density. We conclude and offer our perspectives for the future in Section 4.

2. FORMALISM

In this section, we develop the formalism underpinning covariant DFT and focus on its implementation in the physics of finite nuclei and neutron stars. The Dirac equation obeyed by the nucleon fields and the associated Klein–Gordon equations for the meson fields may be regarded as the generalization of the KS equations to the domain of covariant DFT. As alluded to in Section 1, the effective interaction bears little resemblance to the underlying nucleon–nucleon interaction because the parameters of the model are calibrated to the properties of finite nuclei rather than to two-nucleon data. The application to neutron stars relies on the same EDF without any adjustments. That is, the EoS that serves as the sole input for the Tolman–Oppenheimer–Volkoff (TOV) equations is constructed from the same model that is used to compute the properties of finite nuclei, thereby connecting problems with length scales that differ by about 18 orders of magnitude. Because of space limitations, we omit a discussion of the collective nuclear response, an interesting area of investigation that will continue to thrive with the advent of radioactive beam facilities. For a review of collective excitations in the context of covariant DFT, readers are referred to References 52 and 53 and references contained therein.

2.1. Covariant Density Functional Theory

Finite nuclei are complex many-body systems governed largely by the strong nuclear force. Although quantum chromodynamics (QCD) is the fundamental theory of the strong interaction, many technical hurdles still prevent us from applying QCD in the nonperturbative regime of relevance to nuclear physics. To date, DFT is the most promising—and perhaps only tractable—approach that may be applied over the entire nuclear landscape from finite nuclei to neutron stars. In the traditional nonrelativistic approach, the dynamic information is encoded in an effective interaction between nucleons that is used to build the EDF in terms of conserved isoscalar and isovector (or proton and neutron) densities and their associated currents (21, 22). The paradigm of such an effective nonrelativistic interaction is the Skyrme interaction (17–20). Given that the model parameters cannot be computed from first principles, various optimization protocols are being used to adjust their values by fitting to a suitable set of experimental data (23–25). From such an optimally calibrated density functional, one derives the corresponding KS equations, which are then solved using self-consistent mean-field methods (54).

Covariant DFT follows in the footsteps of Skyrme DFT but with both nucleons and mesons as the fundamental degrees of freedom. Some of the earliest attempts at a relativistic description of the nuclear dynamics include the work of Johnson & Teller (55), Duerr (56), and Miller & Green (57); for a more complete historical account, readers are referred to Reference 58. Besides a desire to understand the saturation of nuclear matter and its impact on the ground-state energy and densities of atomic nuclei, an important motivation for a relativistic description—and one that remains true to this day—was the development of a theory of highly condensed matter that could be applied to the study of neutron stars (59). Originally, quantum hadrodynamics was conceived as a quantum field theory consisting of a nucleon field that interacted via the exchange of neutral scalar and vector mesons (59). Remarkably, a self-consistently generated EoS for

symmetric nuclear matter (SNM) exhibits saturation—even at the mean-field level—because of the different Lorentz character of the scalar and vector interactions. Moreover, pure neutron matter (PNM) was found to be unbound and to remain causal at all densities. However, whereas nuclear saturation—the existence of an equilibrium density at which the pressure vanishes—represented a great triumph of the theory, the curvature around the minimum (i.e., the incompressibility coefficient) was inconsistent with experimental limits obtained from the measurement of the monopole response of heavy nuclei (60). To remedy this deficiency, scalar meson self-interactions, first introduced by Boguta & Bodmer (61), were successful in softening the EoS. Since then, modifications to the underlying effective Lagrangian density have been introduced in an effort to provide a more accurate description of the properties of finite nuclei and neutron stars (37, 58, 62–69). Moreover, some of the most recent parameterizations now provide properly quantified statistical uncertainties.

In the framework of covariant DFT, the basic degrees of freedom are the nucleon (protons and neutrons), three mesons, and the photon. The isodoublet nucleon field ψ interacts via the exchange of photons (A_μ) as well as three massive "mesons": the isoscalar–scalar σ meson, the isoscalar–vector ω meson, and the isovector–vector ρ meson (58, 59, 70). The effective (interacting) Lagrangian density takes the following form (58, 62, 71, 72):

$$\begin{aligned}\mathscr{L}_{\rm int} &= \bar{\psi}\left[g_{\rm s}\phi - \left(g_{\rm v}V_\mu + \frac{g_\rho}{2}\boldsymbol{\tau}\cdot\mathbf{b}_\mu + \frac{e}{2}(1+\tau_3)A_\mu\right)\gamma^\mu\right]\psi \\ &\quad - \frac{\kappa}{3!}(g_{\rm s}\phi)^3 - \frac{\lambda}{4!}(g_{\rm s}\phi)^4 + \frac{\zeta}{4!}g_{\rm v}^4(V_\mu V^\mu)^2 + \Lambda_{\rm v}\left(g_\rho^2\,\mathbf{b}_\mu\cdot\mathbf{b}^\mu\right)\left(g_{\rm v}^2 V_\nu V^\nu\right) \\ &\equiv \bar{\psi}\left[g_{\rm s}\phi - \left(g_{\rm v}V_\mu + \frac{g_\rho}{2}\boldsymbol{\tau}\cdot\mathbf{b}_\mu + \frac{e}{2}(1+\tau_3)A_\mu\right)\gamma^\mu\right]\psi - U_{\rm eff}(\phi, V_\mu, \mathbf{b}_\mu). \qquad 1.\end{aligned}$$

The first line in Equation 1 contains the conventional meson–nucleon Yukawa couplings, while the second line includes nonlinear meson interactions $U_{\rm eff}(\phi, V_\mu, \mathbf{b}_\mu)$ that serve to simulate the complicated many-body dynamics and that are required to improve the predictive power of the model. As alluded to above, the two isoscalar parameters κ and λ introduced by Boguta & Bodmer (61) were designed to reduce the incompressibility coefficient of SNM in accordance with measurements of giant monopole resonances in finite nuclei (60). Sometime later, Müller & Serot (62) introduced the isoscalar parameter ζ to soften the equation of SNM but at much higher densities. They found that by tuning the value of ζ, one could significantly modify the maximum neutron star mass without compromising the success of the model in reproducing ground-state observables. Finally, the mixed isoscalar–isovector parameter $\Lambda_{\rm v}$ was introduced to modify the density dependence of the symmetry energy—particularly its slope at saturation density L. The structure of both neutron-rich nuclei and neutron stars is highly sensitive to the slope of the symmetry energy (71, 73, 74).

The field equations resulting from the above Lagrangian density may be solved exactly in the mean-field limit, where the meson-field operators are replaced by their classical expectation values (58, 59). For a static and spherically symmetric ground state, this implies the following:

$$\phi(x) \to \langle\phi(x)\rangle = \phi_0(r), \qquad 2a.$$

$$V^\mu(x) \to \langle V^\mu(x)\rangle = g^{\mu 0}V_0(r), \qquad 2b.$$

$$b_a^\mu(x) \to \langle b_a^\mu(x)\rangle = g^{\mu 0}\delta_{a3}b_0(r), \qquad 2c.$$

$$A^\mu(x) \to \langle A^\mu(x)\rangle = g^{\mu 0}A_0(r). \qquad 2d.$$

Given that the meson fields couple to their associated bilinear nucleon currents, the baryon sources must also be replaced by their (normal-ordered) expectation values in the mean-field ground state:

$$\bar{\psi}(x)\psi(x) \rightarrow \langle :\bar{\psi}(x)\psi(x):\rangle = \rho_{\rm s}(r), \tag{3a.}$$

$$\bar{\psi}(x)\gamma^{\mu}\psi(x) \rightarrow \langle :\bar{\psi}(x)\gamma^{\mu}\psi(x):\rangle = g^{\mu 0}\rho_{\rm v}(r), \tag{3b.}$$

$$\bar{\psi}(x)\gamma^{\mu}\tau_a\psi(x) \rightarrow \langle :\bar{\psi}(x)\gamma^{\mu}\tau_a\psi(x):\rangle = g^{\mu 0}\delta_{a3}\rho_3(r), \tag{3c.}$$

$$\bar{\psi}(x)\gamma^{\mu}\tau_p\psi(x) \rightarrow \langle :\bar{\psi}(x)\gamma^{\mu}\tau_p\psi(x):\rangle = g^{\mu 0}\rho_p(r), \tag{3d.}$$

where $\rho_{\rm s}$ is the dynamically generated scalar density, $\rho_{\rm v}$ is the conserved isoscalar baryon density, ρ_3 is the isovector baryon density, and ρ_p is the proton density. In terms of the individual proton and neutron densities, one can write $\rho_{\rm v} = \rho_p + \rho_n$ and $\rho_3 = \rho_p - \rho_n$. We have introduced the proton isospin projection operator as $\tau_p = (1 + \tau_3)/2$. Using the above approximations, one can now derive the associated Euler–Lagrangian equations of motion for a generic quantum field q_i (58):

$$\partial_{\mu}\left[\frac{\partial\mathscr{L}}{\partial\left(\partial_{\mu}q_i\right)}\right] - \frac{\partial\mathscr{L}}{\partial q_i} = 0. \tag{4.}$$

In the particular case of the Lagrangian density given in Equation 1, the classical meson fields satisfy Klein–Gordon equations containing both nonlinear meson interactions and ground-state baryon densities as source terms. That is,

$$\left(\nabla^2 - m_{\rm s}^2\right)\phi_0(r) - \frac{\partial U_{\rm eff}}{\partial\phi_0} = -g_{\rm s}\rho_{\rm s}(r), \tag{5a.}$$

$$\left(\nabla^2 - m_{\rm v}^2\right)V_0(r) + \frac{\partial U_{\rm eff}}{\partial V_0} = -g_{\rm v}\rho_{\rm v}(r), \tag{5b.}$$

$$\left(\nabla^2 - m_{\rho}^2\right)b_0(r) + \frac{\partial U_{\rm eff}}{\partial b_0} = -\frac{g_{\rho}}{2}\rho_3(r). \tag{5c.}$$

In turn, the Coulomb field satisfies the much simpler Poisson's equation,

$$\nabla^2 A_0 = -e\rho_p, \tag{6.}$$

while the nucleons satisfy a Dirac equation with the meson fields generating scalar and time-like vector mean-field potentials. That is,

$$\left[-i\boldsymbol{\alpha}\cdot\boldsymbol{\nabla} + g_{\rm v}V_0(r) + \frac{g_{\rho}}{2}\tau_3 b_0(r) + e\tau_p A_0(r) + \beta\Big(M - g_{\rm s}\phi_0(r)\Big)\right]\psi(\mathbf{r}) = E\psi(\mathbf{r}). \tag{7.}$$

The above set of equations—Equations 5–7—represents the effective KS equations for the nuclear many-body problem. As such, this set of mean-field equations must be solved self-consistently. That is, the single-particle orbitals satisfying the Dirac equation are generated from the various meson fields, which in turn satisfy Klein–Gordon equations with the appropriate ground-state densities as the source terms. This process demands an iterative procedure in which mean-field potentials of the Wood–Saxon form are initially provided to solve the Dirac equation for the occupied nucleon orbitals, which are then combined to generate the appropriate densities for the meson field. The Klein–Gordon equations are then solved with the resulting meson fields providing

a refinement to the initial mean-field potentials. This procedure continues until self-consistency is achieved (for a detailed description of the implementation, see Reference 72). Because of the highly nonlinear structure of these equations, extra care must be exercised in ensuring that self-consistency has indeed been achieved.

In the spirit of covariant DFT, the outcomes of the iterative procedure are ground-state densities, binding energies, and self-consistent mean fields. However, given the empirical nature of covariant DFT, one must first adjust the parameters of the interacting density given in Equation 1 to available experimental/observational data. Recently, such a calibrating procedure has been implemented without any reliance on pseudodata—that is, without incorporating assumed bulk properties of infinite nuclear matter (37, 69). Moreover, besides predicting (rather than assuming) the values of several bulk properties of nuclear matter, the statistical approach adopted in the calibrating procedure allows one to provide quantifiable theoretical errors. In doing so, one discovers that the isoscalar sector of the density functional—the sector that does not distinguish neutrons from protons—is fairly well constrained by existing nuclear observables. This is not surprising because most of the experimental nuclear observables available today probe small to moderate neutron–proton asymmetries. In contrast, the isovector sector of the nuclear density functional is poorly constrained. The two isovector parameters defining the effective Lagrangian density in Equation 1 are the Yukawa coupling g_ρ and the mixed isoscalar–isovector coupling Λ_v. As shown in Reference 37, these two model parameters can be fixed once two fundamental parameters of the nuclear symmetry energy have been inferred (see Section 2.3). Enormous theoretical and experimental efforts have been devoted for the last two decades to constraining these two parameters or, more generally, the density dependence of the nuclear symmetry energy. Progress toward achieving this goal by using both laboratory data and astrophysical observables is an important component of this review.

2.2. Neutron Stars

Having explained the main features of the covariant DFT formalism, we now can examine the structure of neutron stars. The structure of spherically symmetric neutron stars in hydrostatic equilibrium—in particular, the fundamental mass-versus-radius relation—is encapsulated in the TOV equations (75, 76). Adopting natural units in which $G = c = 1$, the TOV equations are given by

$$\frac{\mathrm{d}P(r)}{\mathrm{d}r} = -\frac{\Big(\varepsilon(r) + P(r)\Big)\Big(M(r) + 4\pi r^3 P(r)\Big)}{r^2\Big(1 - 2M(r)/r\Big)}, \tag{8a.}$$

$$\frac{\mathrm{d}M(r)}{\mathrm{d}r} = 4\pi r^2 \varepsilon(r). \tag{8b.}$$

Here $M(r)$, $P(r)$, and $\varepsilon(r)$ represent the enclosed mass, pressure, and energy density profiles, respectively. The TOV equations represent the extension of Newtonian gravity to the domain of general relativity. Such extension is essential because the typical escape velocity from the surface of a neutron star is close to the speed of light. Indeed, the Schwarzschild radius of a neutron star (of the order of 3–6 km) is comparable to its 12- to 14-km radius. That is,

$$\frac{v_{\mathrm{esc}}^2}{c^2} = \frac{2GM}{c^2 R} \equiv \frac{R_{\mathrm{s}}(M)}{R}. \tag{9.}$$

Upon inspection, one notices that the only input required for the solution of the TOV equations is an EoS—namely, a relation between the pressure and the energy density. Providing such an

EoS is within the purview of nuclear physics. Although unknown to Oppenheimer & Volkoff at the time of their original contribution (76), the main reason that nuclear physics plays such a predominant role is easy to understand. Back in 1939, Oppenheimer & Volkoff (76) concluded that a neutron star supported exclusively by the quantum pressure from its degenerate neutrons would collapse once its mass exceeded $0.7M_\odot$. Today, however, the evidence for significantly more massive neutron stars is overwhelming (77, 78). Indeed, within the last decade, the existence of three neutron stars with masses in the vicinity of $2M_\odot$ has been firmly established (79–81). In fact, the most massive neutron star observed to date ($M = 2.1^{+0.10}_{-0.09}\,M_\odot$) was reported recently by Cromartie and collaborators (81). This finding implies that the additional support against gravitational collapse must come from nuclear interactions, which at the high densities (or short distances) of the stellar core are known to be strongly repulsive. The large discrepancy between recent observations and the 80-year-old prediction by Oppenheimer & Volkoff (76) has effectively transferred ownership of the neutron star problem to nuclear physics. It is appropriate to mention that unlike the well-known collapse of a white dwarf star, the existence of a maximum neutron star mass is a purely general-relativistic effect with no counterpart in Newtonian gravity. Whereas the collapse of a white dwarf star is characterized by a dramatic reduction in the stellar radius as the mass approaches the Chandrasekhar limit of $M_{\rm Ch} = 1.4M_\odot$ (82), the existence of a maximum neutron star mass develops as an instability against small radial perturbations (83). The maximum neutron star mass is presently unknown, although it has been suggested that GW170817 already provides some important constraints (84).

The existence of neutron stars with masses in excess of $2M_\odot$ demands a stiff EoS—one in which the pressure increases rapidly with energy density. In contrast, the recent detection of gravitational waves from the binary neutron star merger GW170817 suggests that the EoS must be soft. This conclusion was drawn based on the extraction of a rather small value for the tidal deformability (or polarizability) of a $1.4M_\odot$ neutron star (38, 46). The dimensionless tidal deformability is defined as

$$\Lambda = \frac{2}{3}k_2\left(\frac{c^2R}{GM}\right)^5 = \frac{64}{3}k_2\left(\frac{R}{R_{\rm s}}\right)^5, \qquad 10.$$

where k_2 is known as the second Love number (85, 86). Clearly, Λ is extremely sensitive to the compactness parameter $\xi \equiv R_{\rm s}/R$ (87–93). Given that k_2 is known to display a mild sensitivity to the underlying EoS (93), a measurement of Λ, for a given mass, determines the stellar radius and ultimately the stiffness of the EoS.

Trying to account for both large masses and small radii creates an interesting tension that, once resolved, is bound to provide fundamental insights into the EoS. One possibility is that the EoS is relatively soft at about twice nuclear matter saturation density, which is the region believed to be most strongly correlated to the stellar radius (94). In this density domain, the stellar radius is primarily controlled by the density dependence of the nuclear symmetry energy (32, 37, 71, 73, 74). On the other hand, the maximum stellar mass is controlled by the EoS at the highest densities. Thus, one may be able to account for both large masses and small radii if the EoS is soft at intermediate densities and then stiffens at higher densities. Insights into the behavior of the symmetry energy can be gleaned from the recently completed (and currently being analyzed) PREX-II measurement of the neutron skin thickness of ^{208}Pb at Jefferson Lab. It has been demonstrated that the neutron skin thickness of ^{208}Pb is strongly correlated to the slope of the nuclear symmetry energy at saturation density (95–98).

Having established the importance of the tidal polarizability in elucidating the structure of neutron stars, we conclude this section with a brief description of the necessary steps involved in its computation. For simplicity, one can assume that mass, pressure, and energy density profiles

are available after having solved the TOV equations, leaving the second Love number k_2 (85, 86) as the only unknown parameter appearing in Equation 10. Evidently, Λ is extremely sensitive to the compactness parameter ξ (87–92). In turn, the second Love number k_2 depends on both ξ and y_R,

$$k_2(\xi, y_R) = \frac{1}{20}\xi^5(1-\xi)^2\Big[(2-y_R)+(y_R-1)\xi\Big] \times \Big\{\Big[(6-3y_R)+\frac{3}{2}(5y_R-8)\xi\Big]\xi + \frac{1}{2}\Big[(13-11y_R)+\frac{1}{2}(3y_R-2)\xi+\frac{1}{2}(1+y_R)\xi^2\Big]\xi^3 + 3\Big[(2-y_R)+(y_R-1)\xi\Big](1-\xi)^2\ln(1-\xi)\Big\}^{-1}, \quad 11.$$

where $y_R \equiv y(r=R)$ is obtained after solving the following nonlinear, first-order differential equation for $y(r)$—a quantity that is closely related to the tidally induced quadrupole field (90, 91, 93). That is,

$$r\frac{dy(r)}{dr} + y^2(r) + F(r)y(r) + r^2Q(r) = 0, \quad \text{with } y(0)=2. \quad 12.$$

Here the two functions $F(r)$ and $Q(r)$ depend on the known mass, pressure, and energy density profiles of the star:

$$F(r) = \frac{1-4\pi r^2\Big(\varepsilon(r)-P(r)\Big)}{\Big(1-\dfrac{2M(r)}{r}\Big)}, \quad 13a.$$

$$Q(r) = \frac{4\pi}{\Big(1-\dfrac{2M(r)}{r}\Big)}\left(5\varepsilon(r)+9P(r)+\frac{\varepsilon(r)+P(r)}{c_s^2(r)}-\frac{6}{4\pi r^2}\right) - 4\left[\frac{\Big(M(r)+4\pi r^3P(r)\Big)}{r^2\Big(1-\dfrac{2M(r)}{r}\Big)}\right]^2. \quad 13b.$$

In addition, $Q(r)$ depends on the speed-of-sound profile, which involves the derivative of the pressure with respect to the energy density:

$$c_s^2(r) = \frac{dP(r)}{d\varepsilon(r)}. \quad 14.$$

A covariant EDF, unlike nonrelativistic functionals, ensures that the EoS remains causal at all densities—that is, that the speed of sound never exceeds the speed of light.

2.3. Equation of State

Neutron stars are "cold" dense objects with a characteristic core temperature significantly lower than the corresponding Fermi temperature (94, 99). As such, and under the assumption of spherical symmetry and hydrostatic equilibrium, the relevant EoS is that of a zero-temperature, electrically neutral system in chemical (or beta) equilibrium. As we aim to build a covariant EDF that describes the properties of both finite nuclei and neutron stars, we adopt the following as the basic constituents of matter: neutrons, protons, and leptons (both electrons and muons). Leptons help maintain both charge neutrality and beta equilibrium, which ultimately set the proton fraction in the neutron star, a critical property that affects many stellar properties.

Although beta equilibrium dictates that only the total baryon density is conserved, we start with a discussion of the EoS of infinite nuclear matter where both neutron and proton densities are individually conserved. Infinite nuclear matter is an idealized system of protons and neutrons that interact solely via the strong nuclear force, so that both electromagnetic and weak interactions are turned off. In such an idealized situation and under the assumption of translational invariance, the expectation value of the various meson fields in Equation 5 is uniform (i.e., constant throughout space), and the KS orbitals in Equation 7 are plane-wave Dirac spinors with medium-modified effective masses and energies that must be determined self-consistently. To derive the EoS of infinite nuclear matter, one invokes the energy–momentum tensor

$$\mathscr{T}_{\mu\nu} = -g_{\mu\nu}\mathscr{L} + \left[\frac{\partial \mathscr{L}}{\partial\,(\partial^{\mu} q_i)}\right]\partial_{\nu} q_i, \qquad 15.$$

where a sum over all constituent fields q_i is assumed. For a uniform system such as infinite nuclear matter, the expectation value of the energy–momentum tensor takes the following simple form (58):

$$\langle \mathscr{T}_{\mu\nu} \rangle = \Big(\varepsilon + P\Big) u_{\mu} u_{\nu} - P\, g_{\mu\nu}, \qquad 16.$$

where $u^{\mu} = \gamma(1, \boldsymbol{\beta})$ is the scaled four-velocity of the fluid that satisfies the Lorentz-invariant condition $u^2 = u^{\mu} u_{\mu} = 1$, with γ being the Lorentz factor. In particular, for infinite nuclear matter at rest—that is, $u^{\mu} = (1, \mathbf{0})$—it follows that

$$\varepsilon = \langle \mathscr{T}_{00} \rangle \;\text{ and }\; P = \frac{1}{3}\langle \mathscr{T}_{ii} \rangle. \qquad 17.$$

Given that both the proton and neutron densities are conserved in infinite nuclear matter, the EoS at zero temperature may be written as either a function of the individual densities or a function of the total baryon density $\rho = \rho_n + \rho_p$ and the neutron–proton asymmetry $\alpha \equiv (\rho_n - \rho_p)/(\rho_n + \rho_p)$. Expanding the energy per nucleon in even powers of the neutron–proton asymmetry is particularly insightful; that is,

$$\frac{E}{A}(\rho, \alpha) - M \equiv \mathcal{E}(\rho, \alpha) = \mathcal{E}_{\rm SNM}(\rho) + \alpha^2 \mathcal{S}(\rho) + \mathcal{O}(\alpha^4). \qquad 18.$$

Here $\mathcal{E}_{\rm SNM}(\rho) = \mathcal{E}(\rho, \alpha \equiv 0)$ is the energy per nucleon of SNM, and the symmetry energy $\mathcal{S}(\rho)$ represents the first-order correction to the symmetric limit. No odd powers of α appear in the expansion because, in the absence of electroweak interactions, the nuclear force is assumed to be isospin symmetric; isospin violations in the nucleon–nucleon interactions (which are small) are henceforth neglected. Although there is no reason a priori to neglect the higher-order terms in Equation 18, for the models considered in this review the symmetry energy represents to a very good approximation the energy cost required to convert SNM into PNM. That is,

$$\mathcal{S}(\rho) \approx \mathcal{E}(\rho, \alpha = 1) - \mathcal{E}(\rho, \alpha = 0). \qquad 19.$$

While the above relation is model dependent, its validity is easily verified in the case that protons and neutrons behave as noninteracting Fermi gases (100). The separation of the energy per nucleon as in Equation 18 is useful because SNM is sensitive to the isoscalar sector of the density functional, which is well constrained by the properties of stable nuclei. In contrast, the symmetry energy probes the isovector sector of the density functional, which at present is poorly constrained because of the lack of experimental data on very neutron-rich systems. However, this problem will soon be mitigated with the commissioning of radioactive beam facilities throughout the world.

Besides the separation of the EoS into isoscalar and isovector components, it is also useful to characterize the EoS in terms of a few of its bulk parameters defined at saturation density. Nuclear saturation, the existence of an equilibrium density that characterizes the interior of medium to heavy nuclei, is a hallmark of the nuclear dynamics. By performing a Taylor series expansion around nuclear matter saturation density ρ_0 (101), one obtains

$$\mathcal{E}_{\rm SNM}(\rho) = \varepsilon_0 + \frac{1}{2}K_0 x^2 + \ldots, \tag{20a.}$$

$$\mathcal{S}(\rho) = J + Lx + \frac{1}{2}K_{\rm sym}x^2 + \ldots, \tag{20b.}$$

where $x = (\rho - \rho_0)/3\rho_0$ is a dimensionless parameter that quantifies the deviations of the density from its value at saturation. Here ε_0 and K_0 represent the energy per nucleon and the incompressibility coefficient of SNM. The linear term is absent because the pressure of SNM vanishes at saturation density. Thus, the small oscillations around the minimum energy ε_0 are controlled by the incompressibility coefficient K_0. The corresponding quantities in the case of the symmetry energy are denoted by J and $K_{\rm sym}$. However, unlike the case of SNM, the slope of the symmetry energy L does not vanish at saturation density. Indeed, assuming the validity of Equation 19, L is directly proportional to the pressure of PNM at saturation density:

$$P_0 \approx \frac{1}{3}\rho_0 L. \tag{21.}$$

Hence, finding experimental observables that can effectively constrain the slope of the symmetry energy L is tantamount to determining the pressure of a cold neutron gas at saturation density. In Section 3, we explore the predictions of several nuclear density functionals that, while all successful in reproducing a host of laboratory observables, predict significant differences in the properties of neutron-rich systems, such as exotic nuclei and neutron stars.

3. RESULTS

This section is devoted to establishing compelling connections between the properties of finite nuclei and neutron stars. To assess uncertainties in the density dependence of the symmetry energy, we rely on a set of nine successful covariant EDFs. Among them, NL3 (63, 102) and IU-FSU (68) have been used extensively in the literature. In particular, the IU-FSU functional represented an improvement over the original FSUGold model (66) by accounting for the existence of massive neutron stars (79–81). In addition, three different TAMU-FSU models, all with a relatively stiff symmetry energy, were introduced by Fattoyev & Piekarewicz (103) to explore whether existing experimental data could rule out thick neutron skins in ^{208}Pb. The remaining density functionals were calibrated for the first time using exclusively physical observables (37, 69). That is, unlike earlier approaches, bulk properties of infinite nuclear matter were now predicted rather than assumed. Moreover, the calibration protocol relied on a statistically robust covariance analysis that provided both theoretical uncertainties and correlation coefficients (37). The only significant difference in the calibration of these functionals was an assumed value for the presently unknown neutron skin thickness of ^{208}Pb (69).

3.1. Ground-State Properties

To assess the performance of the nine models employed in this review, we display in **Figure 1** theoretical predictions relative to experiment for the binding energies per nucleon (104) and charge

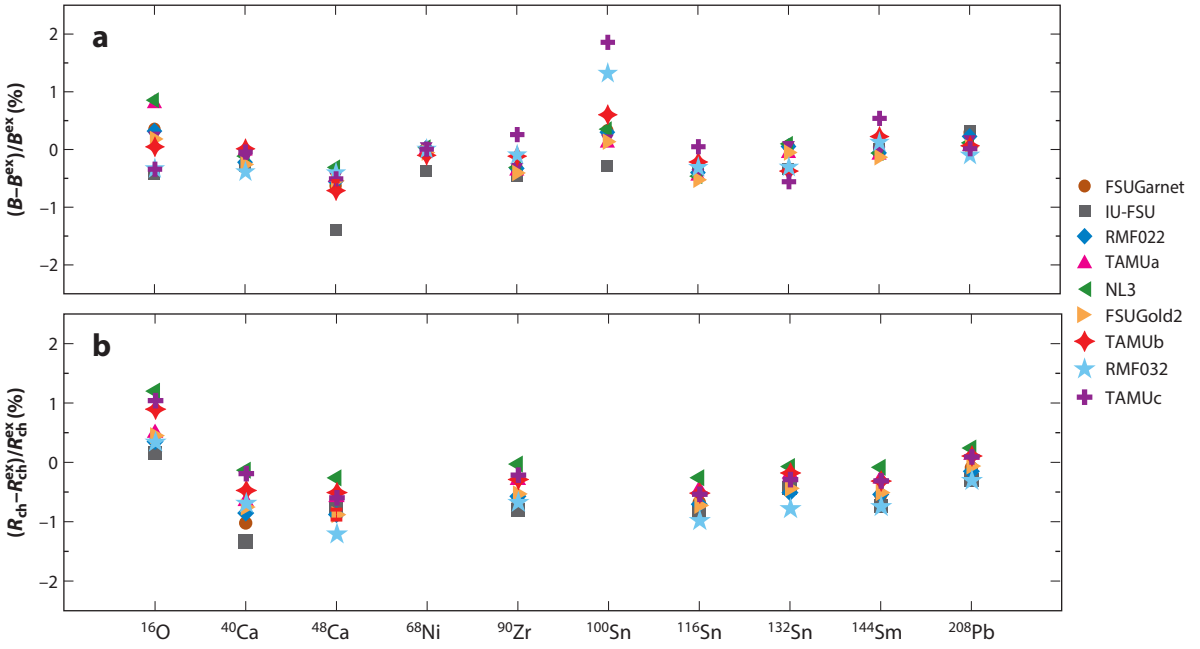

Figure 1

Comparison between the theoretical predictions of nine successful covariant energy density functional models for (*a*) the binding energy and (*b*) the charge radius of a representative set of magic and semimagic nuclei. Results are shown as percent fractional discrepancy.

radii (105) of a representative set of magic and semimagic nuclei. In all cases, the predictions fall within 2% of the experimental values. However, it is worth mentioning that for most of these functionals, the binding energies and charge radii displayed in the figure were incorporated into the fitting protocol. Nevertheless, these results suggest that extrapolations to the high-density regime characteristic of neutron stars involve covariant EDFs that are consistent with known properties of finite nuclei.

3.2. Neutron Star Properties

Although both relativistic and nonrelativistic EDFs have been enormously successful in describing ground-state properties of finite nuclei and their collective response, there is a distinct advantage in using a Lorentz covariant formulation as one extrapolates to dense nuclear matter. Inherent to any consistent relativistic framework is the observance of "causality"—namely, the fact that no signal can propagate faster than the speed of light. In the context of dense matter, this implies a limit to the stiffness of the EoS given by $P \leq \varepsilon$, which in the context of Equation 14 implies that the speed of sound remains below the speed of light at all densities. However, the causal limit is often violated in nonrelativistic descriptions, especially as central densities become large enough to support $2M_{\odot}$ neutron stars. Violating causality is particularly problematic in the case of the tidal polarizability because the relevant differential equation depends explicitly on the speed of sound (see Equation 13b).

Predictions for the EoS of SNM and the symmetry energy are displayed in **Figure 2**. Under the assumption that Equation 19 is valid, the EoS of PNM (not shown) is approximately equal to the sum of these two contributions. In the case of SNM, all models predict a saturation point

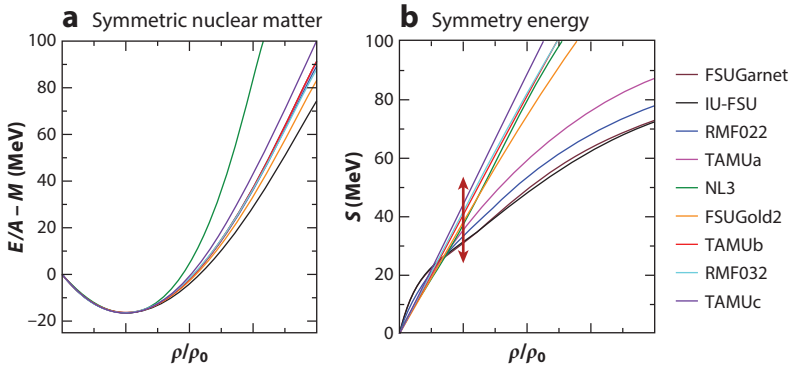

Figure 2

Binding energy per nucleon (*a*) and nuclear symmetry energy (*b*) as a function of the baryon density as predicted by nine successful covariant energy density functional models. The arrow in panel *b* indicates the large model spread in the slope of the symmetry energy at saturation density.

located at $\rho_0 \approx 0.15$ fm^{-3} and a binding energy per nucleon of $\varepsilon_0 \approx -16$ MeV. We use the word predict because many of these functionals were calibrated using exclusively physical observables; no bulk properties of nuclear matter were incorporated into the calibration procedure (37, 69). This agreement among the models suggests that the values commonly adopted for both ρ_0 and ε_0 are properly encoded in certain bulk properties of finite nuclei.

Beyond the saturation point, the small oscillations around the minimum are controlled by the incompressibility coefficient K_0. Experimental measurements of the giant monopole resonance in ^{208}Pb—and also on a few lighter nuclei, such as ^{144}Sm and ^{90}Zr—have constrained K_0 to a range of 240 ± 20 MeV (see Reference 106 and references contained therein). The NL3 model (shown in green in **Figure 2**) was conceived before such stringent constraints were available, leading to a large incompressibility coefficient K_0 that, in turn, generates a very stiff EoS for SNM. In contrast, some of the most recently calibrated functionals have incorporated for the first time information on giant monopole energies. As such, the incompressibility coefficient predicted by these models is fully consistent with experiment (37). However, measurements of the distribution of isoscalar monopole strength in the isotopic chains of both tin and cadmium seem to suggest a smaller value for K_0 (107, 108). After more than a decade, the issue of the softness (or "fluffiness") of these open-shell nuclei remains unresolved (109, 110).

Whereas ground-state properties and collective excitations of finite nuclei impose stringent constraints on the behavior of SNM, at present, these properties do not significantly constrain the symmetry energy (see **Figure 2*b***). It appears that nuclear ground-state properties, in particular the masses of neutron-rich nuclei, determine rather accurately the value of the symmetry energy at about two-thirds of nuclear matter saturation density—that is, at $\rho \approx (2/3)\rho_0 \approx 0.1$ fm^{-3} (71, 95, 96, 111, 112). However, the slope of the symmetry energy in the vicinity of saturation density is poorly constrained by nuclear observables. To mitigate this problem, the neutron skin thickness of ^{208}Pb was identified as an ideal proxy for L. Indeed, a very strong correlation was found between L and the neutron skin thickness of ^{208}Pb (95–98). Given that SNM saturates, the slope of the symmetry energy L is directly related to the pressure of PNM at saturation density (see Equation 21). As a result, measurement of the neutron skin thickness of ^{208}Pb provides critical information on a fundamental parameter of the EoS. Motivated by this finding, the lead radius experiment (PREX) at Jefferson Lab was commissioned about a decade ago and has already provided the first model-independent evidence in favor of a neutron-rich skin in ^{208}Pb (113, 114). Unfortunately,

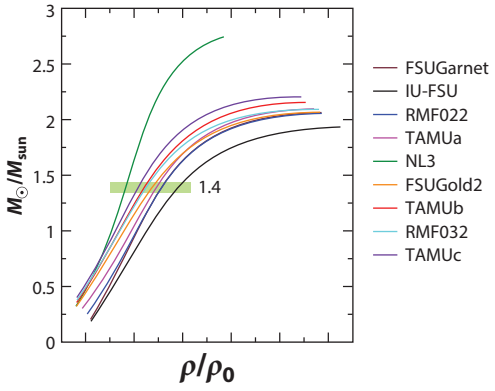

Figure 3

Relationship between the mass of a neutron star and the central density required to support such a star as predicted by nine successful covariant energy density functional models. The green bar illustrates the significant model dependence on the central density required to support a $1.4M_\odot$ neutron star.

because of unanticipated experimental challenges, PREX was not able to reach its original goal of a 1% determination of the neutron radius of ^{208}Pb. Since then, the follow-up PREX-II campaign has been successfully completed, and CREX was commissioned at the time of this writing (*6*). In conjunction, PREX-II and CREX will provide valuable information on the EoS of neutron-rich matter. Until then, one must explore how the uncertainties in the density dependence of the symmetry energy affect our predictions regarding the properties of neutron stars.

Although PREX-II and CREX constrain the behavior of neutron-rich matter in the vicinity of nuclear matter saturation density, neutron stars are sensitive to the EoS up to several times saturation density. To assess the range of densities probed in the interior of neutron stars, we display in **Figure 3** the central density required to support a neutron star of a given mass. As expected, the required central density depends critically on the stiffness of the EoS. For example, in the case of NL3—the model with the stiffest EoS—the central density lies below $4\rho_0$ for all masses below its predicted maximum mass of $\sim 2.7M_\odot$. In contrast, the IU-FSU model with the softest EoS requires a central density in excess of $6\rho_0$ to support a maximum mass of $\lesssim 2M_\odot$. These densities may get even higher in the event of a phase transition in the stellar core—a situation that we do not contemplate in this contribution. Finally, the green bar in **Figure 3** illustrates the model dependence on the central density that is required to support a canonical $1.4M_\odot$ neutron star: from less than twice ρ_0 (for NL3) to about three times ρ_0 (for IU-FSU).

Stellar radii seem to be largely determined by the density dependence of the symmetry energy in the immediate vicinity of nuclear matter saturation density. Indeed, it has been argued that the pressure near twice saturation density sets the overall scale for stellar radii (94). This line of argument suggests that although PREX-II cannot determine the stiffness of the EoS at high densities, it should provide valuable insights into the overall size of neutron stars (71, 73). To underscore the strong correlation between the slope of the symmetry energy L and the radius of a $1.4M_\odot$ neutron star, we display in **Figure 4*a*** 39% and 95% confidence ellipses using the FSUGold2 density functional as an example. FSUGold2 is particularly convenient to illustrate this correlation because no biases were introduced in the calibration of the functional—particularly in connection to the (presently unknown) neutron skin thickness of ^{208}Pb (37). With a correlation coefficient of almost one ($\rho = 0.995$) and nearly "degenerate" ellipses, a nearly one-to-one correspondence exists between L and $R_{1.4}$. Given that the neutron skin thickness of ^{208}Pb provides an ideal proxy

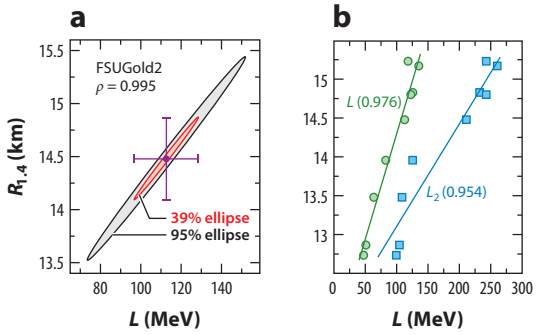

Figure 4

(*a*) The 39% and 95% confidence ellipses between the slope of symmetry energy L and the radius of a $1.4M_\odot$ neutron star as predicted by the FSUGold2 density functional. Also displayed in panel *a* are the corresponding statistical errors in L and $R_{1.4}$. (*b*) Systematic uncertainties in the same correlation but now as predicted by nine successful covariant energy density functional models. Also shown in panel *b* is the correlation between L_2 (the slope of the symmetry energy at twice saturation density) and $R_{1.4}$.

for L, a powerful data-to-data relation emerges between neutron-rich systems—finite nuclei and neutron stars—that differ in size by 18 orders of magnitude.

Although the correlation displayed in **Figure 4*a*** is compelling, the statistical analysis carried out is unable to assess systematic errors associated with the intrinsic limitations of a given model—in this case, FSUGold2. To properly assess systematic uncertainties, we include in **Figure 4*b*** the predictions of each of the nine models considered in this review. Although slightly weaker ($\rho = 0.976$) than in **Figure 4*a***, the correlation between L and $R_{1.4}$ remains very strong. However, the correlation between $R_{1.4}$ and the slope of the symmetry energy at twice saturation density (L_2) appears slightly weaker. In light of the expectation that stellar radii are sensitive to the density dependence of the symmetry energy near twice saturation density (94), our finding is mildly surprising, so it should be examined within the context of a more diverse set of EDFs.

We close this section by addressing the recent excitement in the field prompted by the historic detection of gravitational waves from the binary neutron star merger GW170817 (38). Unlike earlier detections of black hole mergers that emitted no electromagnetic radiation (115), GW170817 opened a new era of multimessenger astronomy. Indeed, the gravitational wave signal triggered public alerts that enabled myriad telescopes operating at all wavelengths to follow the electromagnetic counterpart (39–42), a critical fact in establishing binary neutron star mergers as favorable sites for the formation of the heavy elements. **Figure 5*a*** shows predictions for the dimensionless tidal polarizability Λ of a $1.4M_\odot$ neutron star as a function of the stellar radius (44, 116, 117). Given the strong sensitivity of Λ to the stellar compactness as indicated in Equation 10, the displayed correlation is very strong once the stellar mass has been fixed. Indeed, since k_2 is known to display a mild sensitivity to the underlying EoS (93), the curve fitted to the theoretical predictions scales approximately with the fifth power of the radius (44).

The extraction of the tidal polarizability of a $1.4M_\odot$ neutron star provides the strongest constraint from GW170817 on the EoS of neutron-rich matter. In the initial discovery paper (38), the LIGO-Virgo collaboration placed a 90% upper bound of $\Lambda_{1.4} \leq 800$ that was strict enough to disfavor overly stiff EoSs (44, 45). Since then, some of the initial assumptions have been relaxed, leading to the more stringent upper limit of $\Lambda_{1.4} = 190^{+390}_{-120}$, which implies a common radius for the two colliding neutron stars of $R = 11.9 \pm 1.4$ km (46). As illustrated in **Figure 5*a***, this revised

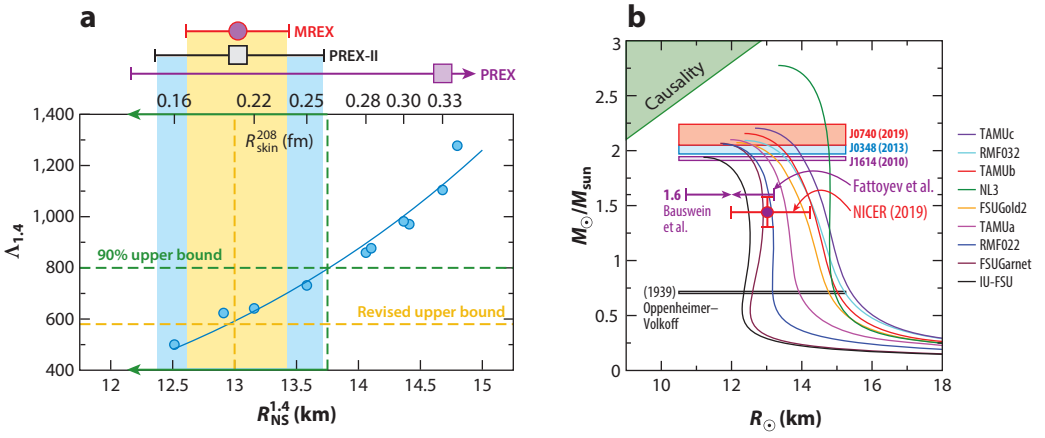

Figure 5

(*a*) Tidal polarizability of a $1.4M_\odot$ neutron star as a function of both the stellar radius and the neutron skin thickness of ^{208}Pb. Shown in the upper abscissa is the PREX result with its associated large error bar (113, 114), alongside the anticipated more precise determinations from PREX-II and MREX (116). Although the error bars are realistic, the central values are placed arbitrarily at $R^{208}_{skin} \simeq 0.2$ fm. (*b*) The mass-versus-radius relation as predicted by nine successful covariant energy density functional models, together with limits extracted from theory, electromagnetic observations, and gravitational wave detections (43–45, 76, 79–81, 118). Abbreviation: NICER, Neutron Star Interior Composition Explorer.

upper bound creates enormous tension as it excludes most theoretical models—even when all the models provide an excellent description of the ground-state properties of finite nuclei.

The tension is further exacerbated as one examines masses and radii simultaneously. The characteristic mass–radius relation as predicted by the nine models used in this review is displayed in **Figure 5*b***. In addition to these nine theoretical predictions, the figure includes several interesting limits. The 1939 prediction by Oppenheimer & Volkoff (76) for the maximum neutron star mass—assuming that the entire pressure support is due to a noninteracting Fermi gas of neutrons—is displayed in the lower part of the figure. This pioneering prediction has long been refuted, especially with the confirmation of three neutron stars with masses in the vicinity of $2M_\odot$ (79–81) (see the three bars in the upper portion of **Figure 5*b***). For instance, Cromartie and collaborators (81) have measured a neutron star with a mass of about $2.14M_\odot$—a value that is tantalizingly close to the upper limit of $M_{max} = 2.17M_\odot$ suggested by Margalit & Metzger (84) from exploiting the multimessenger nature of GW170817. By also combining gravitational wave and electromagnetic information from GW170817, Bauswein and collaborators (43) have provided a lower limit on the radius of a $1.6M_\odot$ neutron star, which, when combined with the upper limits obtained by Fattoyev et al. (44) and Annala et al. (45), results in the two arrows facing each other in **Figure 5*b***. Finally, the figure includes results from the very recent simultaneous extraction of the mass and radius of PSR J0030+0451 by the Neutron Star Interior Composition Explorer (NICER). The quoted results by Miller and collaborators (118) are $M = 1.44^{+0.15}_{-0.14}M_\odot$ and $R = 13.02^{+1.24}_{-1.06}M_\odot$. These values are consistent with the independent analysis reported by Riley and collaborators (119). Although the first NICER results do not impose stringent constraints on the EoS, this pioneering measurement has determined for the first time the gravitational mass and equatorial radius of a neutron star.

So what do we conclude? On the one hand, the existence of massive neutron stars suggests that the EoS at high densities must be relatively stiff to provide the necessary pressure support. On the other hand, GW170817 seems to favor compact stars with small radii—suggesting instead

that the EoS must be soft. How can we then simultaneously account for both small radii and large masses? As argued earlier, stellar radii appear to be sensitive to the EoS of neutron-rich matter in the vicinity of nuclear matter saturation density. In contrast, the maximum neutron star mass is sensitive to the EoS at the highest densities attained in the stellar core. Hence, the apparent tension may be resolved if the EoS is soft at intermediate densities—thereby accounting for the small radii—but then stiffens at higher densities to support heavy neutron stars. This already-unique situation could become even more interesting if PREX-II confirms the original PREX measurement of a neutron skin thickness of $R_{\rm skin}^{208} = 0.33$ fm, albeit with larger error bars (113, 114). If confirmed, this finding would imply that the EoS is stiff in the vicinity of saturation density, that it will then soften at intermediate densities to account for the small stellar radii, and that it will ultimately stiffen at high densities, thus explaining the existence of massive neutron stars. The evolution from stiff to soft and back to stiff may reflect fascinating underlying dynamics, perhaps indicative of an exotic phase transition in the stellar interior.

4. CONCLUSIONS

Nuclear science is driven by the quest to understand the fundamental interactions that shape the structure of the universe. A new generation of terrestrial facilities being commissioned all over the world will help answer some key science questions, such as, How did visible matter come into being and how does it evolve, and how does subatomic matter organize itself and what phenomena emerge (1)? Insights into the dynamics of neutron-rich matter will emerge from the study of exotic nuclei with very large neutron skins. In the cosmos, neutron-rich matter is at the heart of many fundamental questions, such as, What are the new states of matter at exceedingly high density and temperature? And how were the elements from iron to uranium made (120)? Remarkable developments that have occurred within the last few years are providing valuable insights into the nature of dense neutron-rich matter. First, the direct detection of gravitational waves from the binary neutron star merger GW170817 suggests that neutron stars are fairly compact, implying a relatively soft EoS at intermediate densities (38). Second, the observation by Cromartie and collaborators (81) of the most massive neutron star to date implies that the EoS must stiffen at high densities. Finally, NICER—aboard the International Space Station—has reported the very first simultaneous measurement of the mass and radius of a neutron star (118, 119). This pioneering result is highly significant because a one-to-one correspondence exists between the mass–radius relation of neutron stars and the underlying EoS (121).

As we embark on this new journey of discovery, nuclear theory will play a critical role in guiding new experimental programs and will continue to make predictions in regimes that remain inaccessible to experiment and observation. Prospects in nuclear theory are excellent given the recent advances in ab initio methods that start from chiral effective field theory Hamiltonians fitted to two- and three-body data (8). Indeed, within the last decade, ab initio calculations have seen an explosive growth in scalability to larger systems. Yet despite this undeniable progress, DFT remains the most promising and only tractable approach that may be applied over the entire nuclear landscape from finite nuclei to neutron stars. The main goal of this review is to demonstrate the power and flexibility of modern covariant EDFs in predicting the properties of nuclear systems across such a rich and diverse landscape. Particularly important in this context is the unique synergy between nuclear physics and astrophysics in the brand new era of gravitational wave astronomy.

So what is the path forward in the development of DFT as it pertains to nuclear physics? Perhaps the most serious obstacle is the lack of a one-to-one correspondence between the one-body nuclear density and a suitable external potential—a requirement that is germane to DFT as originally conceived by Hohenberg & Kohn (9, 10). Moreover, unlike DFT applications to

electronic structure where the fundamental interaction is known, the underlying nucleon–nucleon interaction—although often inspired by QCD—relies on fits to two- and three-nucleon data. A much more fruitful application of DFT to nuclear physics is through the KS equations, a set of equations that is highly reminiscent of the traditional mean-field approach that lies at the heart of nuclear physics. However, in contrast to the KS formalism that yields in principle the exact ground-state energy and one-body density, no such guarantee exists in nuclear physics because the universal nuclear mean-field potential is unknown. Nevertheless, enormous progress in ab initio approaches provides meaningful benchmarks for the refinement of existing nuclear functionals. The CREX campaign at Jefferson Lab was motivated in part by the powerful connection between ab initio approaches and DFT (6, 7). Finally, nuclear density functionals will be informed and refined by the wealth of experimental and observational data that will emerge from rare isotope facilities, telescopes operating across the entire electromagnetic spectrum, and ever more sensitive gravitational wave detectors. This unique synergy will prove vital in our quest to determine the nuclear EoS.

DISCLOSURE STATEMENT

The authors are not aware of any affiliations, memberships, funding, or financial holdings that might be perceived as affecting the objectivity of this review.

ACKNOWLEDGMENTS

This material is based on work supported by the US Department of Energy Office of Science, Office of Nuclear Physics (award DE-FG02-92ER40750).

LITERATURE CITED

1. Geesaman D, et al. *Reaching for the horizon: the 2015 long range plan for nuclear science*. Rep., US Dep. Energy, Washington, DC. **http://inspirehep.net/record/1398831/files/2015_LRPNS_091815.pdf** (2015)
2. Pieper SC, Wiringa RB. *Annu. Rev. Nucl. Part. Sci.* 51:53 (2001)
3. Barrett BR, Navratil P, Vary JP. *Prog. Part. Nucl. Phys.* 69:131 (2013)
4. Hagen G, Papenbrock T, Hjorth-Jensen M, Dean DJ. *Rep. Prog. Phys.* 77:096302 (2014)
5. Navratil P, et al. *Phys. Scr.* 91:053002 (2016)
6. Mammei J, et al. *CREX: parity-violating measurement of the weak-charge distribution of ^{48}Ca*. Hall A Collab. Propos., Jefferson Lab, Newport News, VA. **https://hallaweb.jlab.org/parity/prex/c-rex2013_v7.pdf** (2013)
7. Horowitz CJ, Kumar KS, Michaels R. *Eur. Phys. J. A* 50:48 (2014)
8. Furnstahl RJ. arXiv:1906.00833 [nucl-th] (2019)
9. Hohenberg P, Kohn W. *Phys. Rev.* 136:B864 (1964)
10. Kohn W, Sham LJ. *Phys. Rev.* 140:A1133 (1965)
11. Kohn W. *Rev. Mod. Phys.* 71:1253 (1999)
12. Fiolhais C, Nogueira F, Marques M. *A Primer in Density Functional Theory*. Berlin: Springer-Verlag (2003)
13. Burke K. *The ABC of DFT*. Work. Pap., Dep. Chem., Univ. Calif., Irvine. **https://dft.uci.edu/doc/g1.pdf** (2007)
14. Skylaris CK. *DFT lectures*. **https://www.southampton.ac.uk/compchem/people/teaching.page** (2020)
15. Drut JE, Furnstahl RJ, Platter L. *Prog. Part. Nucl. Phys.* 64:120 (2010)
16. Negele JW. *Rev. Mod. Phys.* 54:913 (1982)
17. Skyrme THR. *Philos. Mag.* 1:1043 (1956)
18. Skyrme T. *Nucl. Phys.* 9:615 (1959)

19. Vautherin D, Brink DM. *Phys. Rev. C* 5:626 (1972)
20. Stone JR, Reinhard PG. *Prog. Part. Nucl. Phys.* 58:587 (2007)
21. Bertsch GF. *J. Phys. Conf. Ser.* 78:012005 (2007)
22. Stoitsov M, et al. *J. Phys. Conf. Ser.* 180:012082 (2009)
23. Kortelainen M, et al. *Phys. Rev. C* 82:024313 (2010)
24. Erler J, et al. *Nature* 486:509 (2012)
25. Kortelainen M, et al. *Phys. Rev. C* 89:054314 (2013)
26. Thouless D. *Nucl. Phys.* 22:78 (1961)
27. Dawson JF, Furnstahl RJ. *Phys. Rev. C* 42:2009 (1990)
28. Horowitz CJ, Piekarewicz J. *Phys. Rev. C* 64:062802(R) (2001)
29. Ring P, Schuck P. *The Nuclear Many-Body Problem*. New York: Springer (2004)
30. Fattoyev F, Piekarewicz J. *Phys. Rev. C* 84:064302 (2011)
31. Reinhard PG, Nazarewicz W. *Phys. Rev. C* 81:051303 (2010)
32. Fattoyev F, Piekarewicz J. *Phys. Rev. C* 86:015802 (2012)
33. Reinhard P, Nazarewicz W. *Phys. Rev. C* 87:014324 (2013)
34. Reinhard PG, et al. *Phys. Rev. C* 88:034325 (2013)
35. Dobaczewski J, Nazarewicz W, Reinhard PG. *J. Phys. G* 41:074001 (2014)
36. Piekarewicz J, Chen WC, Fattoyev F. *J. Phys. G* 42:034018 (2015)
37. Chen WC, Piekarewicz J. *Phys. Rev. C* 90:044305 (2014)
38. Abbott BP, et al. *Phys. Rev. Lett.* 119:161101 (2017)
39. Drout MR, et al. *Science* 358:1570 (2017)
40. Cowperthwaite PS, et al. *Astrophys. J.* 848:L17 (2017)
41. Chornock R, et al. *Astrophys. J.* 848:L19 (2017)
42. Nicholl M, et al. *Astrophys. J.* 848:L18 (2017)
43. Bauswein A, Just O, Janka HT, Stergioulas N. *Astrophys. J.* 850:L34 (2017)
44. Fattoyev FJ, Piekarewicz J, Horowitz CJ. *Phys. Rev. Lett.* 120:172702 (2018)
45. Annala E, Gorda T, Kurkela A, Vuorinen A. *Phys. Rev. Lett.* 120:172703 (2018)
46. Abbott BP, et al. *Phys. Rev. Lett.* 121:161101 (2018)
47. Most ER, Weih LR, Rezzolla L, Schaffner-Bielich J. *Phys. Rev. Lett.* 120:261103 (2018)
48. Tews I, Margueron J, Reddy S. *Phys. Rev. C* 98:045804 (2018)
49. Malik T, et al. *Phys. Rev. C* 98:035804 (2018)
50. Tsang CY, et al. arXiv:1807.06571 [nucl-ex] (2018)
51. Radice D, Dai L. *Eur. Phys. J. A* 55:50 (2019)
52. Piekarewicz J. *Eur. Phys. J. A* 50:25 (2013)
53. Piekarewicz J. *Int. J. Mod. Phys. E* 24:1541003 (2015)
54. Bender M, Heenen PH, Reinhard PG. *Rev. Mod. Phys.* 75:121 (2003)
55. Johnson MH, Teller E. *Phys. Rev.* 98:783 (1955)
56. Duerr HP. *Phys. Rev.* 103:469 (1956)
57. Miller LD, Green AES. *Phys. Rev. C* 5:241 (1972)
58. Serot BD, Walecka JD. *The Relativistic Nuclear Many-Body Problem*. New York: Plenum (1986)
59. Walecka JD. *Ann. Phys.* 83:491 (1974)
60. Youngblood DH, et al. *Phys. Rev. Lett.* 39:1188 (1977)
61. Boguta J, Bodmer AR. *Nucl. Phys. A* 292:413 (1977)
62. Müller H, Serot BD. *Nucl. Phys. A* 606:508 (1996)
63. Lalazissis GA, Konig J, Ring P. *Phys. Rev. C* 55:540 (1997)
64. Vretenar D, Niksic T, Ring P. *Phys. Rev. C* 68:024310 (2003)
65. Lalazissis GA, Niksic T, Vretenar D, Ring P. *Phys. Rev. C* 71:024312 (2005)
66. Todd-Rutel BG, Piekarewicz J. *Phys. Rev. Lett.* 95:122501 (2005)
67. Agrawal B. *Phys. Rev. C* 81:034323 (2010)
68. Fattoyev FJ, Horowitz CJ, Piekarewicz J, Shen G. *Phys. Rev. C* 82:055803 (2010)
69. Chen WC, Piekarewicz J. *Phys. Lett. B* 748:284 (2015)
70. Serot BD, Walecka JD. *Int. J. Mod. Phys. E* 6:515 (1997)

71. Horowitz CJ, Piekarewicz J. *Phys. Rev. Lett.* 86:5647 (2001)
72. Todd BG, Piekarewicz J. *Phys. Rev. C* 67:044317 (2003)
73. Horowitz CJ, Piekarewicz J. *Phys. Rev. C* 64:062802 (2001)
74. Carriere J, Horowitz CJ, Piekarewicz J. *Astrophys. J.* 593:463 (2003)
75. Tolman RC. *Phys. Rev.* 55:364 (1939)
76. Oppenheimer JR, Volkoff GM. *Phys. Rev.* 55:374 (1939)
77. Thorsett S, Chakrabarty D. *Astrophys. J.* 512:288 (1999)
78. Lattimer JM, Prakash M. *Science* 304:536 (2004)
79. Demorest P, et al. *Nature* 467:1081 (2010)
80. Antoniadis J, et al. *Science* 340:6131 (2013)
81. Cromartie HT, et al. *Nat. Astron.* 4:72 (2019)
82. Chandrasekhar S. *Astrophys. J.* 74:81 (1931)
83. Weinberg S. *Gravitation and Cosmology*. New York: John Wiley & Sons (1972)
84. Margalit B, Metzger BD. *Astrophys. J.* 850:L19 (2017)
85. Binnington T, Poisson E. *Phys. Rev. D* 80:084018 (2009)
86. Damour T, Nagar A, Villain L. *Phys. Rev. D* 85:123007 (2012)
87. Hinderer T. *Astrophys. J.* 677:1216 (2008)
88. Hinderer T, Lackey BD, Lang RN, Read JS. *Phys. Rev. D* 81:123016 (2010)
89. Damour T, Nagar A. *Phys. Rev. D* 80:084035 (2009)
90. Postnikov S, Prakash M, Lattimer JM. *Phys. Rev. D* 82:024016 (2010)
91. Fattoyev FJ, Carvajal J, Newton WG, Li BA. *Phys. Rev. C* 87:015806 (2013)
92. Steiner AW, Gandolfi S, Fattoyev FJ, Newton WG. *Phys. Rev. C* 91:015804 (2015)
93. Piekarewicz J, Fattoyev FJ. *Phys. Rev. C* 99:045802 (2019)
94. Lattimer JM, Prakash M. *Phys. Rep.* 442:109 (2007)
95. Brown BA. *Phys. Rev. Lett.* 85:5296 (2000)
96. Furnstahl RJ. *Nucl. Phys. A* 706:85 (2002)
97. Centelles M, Roca-Maza X, Viñas X, Warda M. *Phys. Rev. Lett.* 102:122502 (2009)
98. Roca-Maza X, Centelles M, Viñas X, Warda M. *Phys. Rev. Lett.* 106:252501 (2011)
99. Page D, Reddy S. *Annu. Rev. Nucl. Part. Sci.* 56:327 (2006)
100. Piekarewicz J. *Neutron Star Matter Equation of State*. Cham, Switz.: Springer Int. (2017)
101. Piekarewicz J, Centelles M. *Phys. Rev. C* 79:054311 (2009)
102. Lalazissis GA, Raman S, Ring P. *At. Data Nucl. Data Tables* 71:1 (1999)
103. Fattoyev FJ, Piekarewicz J. *Phys. Rev. Lett.* 111:162501 (2013)
104. Huang WJ, et al. *Chin. Phys. C* 41:030002 (2017)
105. Angeli I, Marinova K. *At. Data Nucl. Data Tables* 99:69 (2013)
106. Garg U, Coló G. *Prog. Part. Nucl. Phys.* 101:55 (2018)
107. Li T, et al. *Phys. Rev. Lett.* 99:162503 (2007)
108. Patel D, et al. *Phys. Lett. B* 718:447 (2012)
109. Garg U, et al. *Nucl. Phys. A* 788:36 (2007)
110. Piekarewicz J. *Phys. Rev. C* 76:031301 (2007)
111. Ducoin C, Margueron J, Providencia C, Vidana I. *Phys. Rev. C* 83:045810 (2011)
112. Horowitz CJ, et al. *J. Phys. G* 41:093001 (2014)
113. Abrahamyan S, et al. *Phys. Rev. Lett.* 108:112502 (2012)
114. Horowitz CJ, et al. *Phys. Rev. C* 85:032501 (2012)
115. Abbott BP, et al. *Phys. Rev. Lett.* 116:061102 (2016)
116. Thiel M, et al. *J. Phys. G* 46:093003 (2019)
117. Piekarewicz J, Fattoyev FJ. *Phys. Today* 72:30 (2019)
118. Miller MC, et al. *Astrophys. J. Lett.* 887:L24 (2019)
119. Riley TE, et al. *Astrophys. J. Lett.* 887:L21 (2019)
120. Turner MS, et al. *Connecting Quarks with the Cosmos: Eleven Science Questions for the New Century*. Washington, DC: Natl. Acad. Press (2003)
121. Lindblom L. *Astrophys. J.* 398:569 (1992)

Annual Review of Nuclear and Particle Science

Volume 70, 2020

Contents

Errata

An online log of corrections to *Annual Review of Nuclear and Particle Science* articles may be found at http://www.annualreviews.org/errata/nucl